Onboard Real-Time Absolute Radiometric Calibration for Thermal Infrared Channels of Chinese Geostationary Meteorological Satellites

JINJUN TONG

Environmental Science and Engineering Program, University of Northern British Columbia, Prince George, British Columbia, Canada, and Key Laboratory of Radiometric Calibration and Validation for Environmental Satellites, China Meteorological Administration, National Satellite Meteorology Center, Beijing, China

STEPHEN J. DÉRY

Environmental Science and Engineering Program, University of Northern British Columbia, Prince George, British Columbia, Canada

BO HU

Department of Human Resources, China Meteorological Administration, Beijing, China

YUN CHEN

National Meteorological Centre, China Meteorological Administration, Beijing, China

CHANGJUN YANG AND ZHIGUO RONG

Key Laboratory of Radiometric Calibration and Validation for Environmental Satellites, China Meteorological Administration, National Satellite Meteorology Center, Beijing, China

(Manuscript received 12 March 2008, in final form 25 June 2008)

ABSTRACT

Forty-one cloud-free images of Qinghai Lake (QHL) in China and the corresponding digital numbers (DNs) of FengYun-2C (FY-2C) at 0000, 0600, 1200, and 1800 UTC from 1 July to 30 September 2005 are analyzed. The corresponding surface water temperatures of QHL measured by the automated hydrometeorological buoy (AHMB) system and the atmospheric profiles over QHL from the National Centers for Environmental Prediction (NCEP) reanalysis data are inputted into the atmospheric transfer model MODTRAN3.7 to calculate the entrance pupil radiance and brightness temperatures for thermal infrared (TIR) channels of FY-2C. Then, the absolute radiometric calibration coefficients of FY-2C, which are used to calculate the equivalent blackbody (EBB) temperatures T_{EBB}, are calculated by comparing the entrance pupil radiance and brightness temperatures with the corresponding DNs. In addition, the temperatures of onboard blackbody (OBB) T_{OBB}, primary, secondary, refraction, and calibration mirrors on the multichannel scanning radiometer (MSR) of FY-2C are detected remotely. Based on the linear correlation between $T_{\mathrm{EBB}} - T_{\mathrm{OBB}}$ and temperatures of various mirrors, the transform equations from T_{OBB} to T_{EBB} are developed. Finally, the onboard real-time absolute radiometric calibration for TIR channels of geostationary meteorological satellite FY-2C is implemented with an uncertainty of about 1.5 and 2.1 K for TIR 1 and TIR 2 of FY-2C, respectively.

1. Introduction

The thermal infrared (TIR) channels of remote platforms are comprehensively applied to study such phenomena as urban heat island effects, to classify cloud types, and to track sea, land, and snow surface temperatures. The accuracy of the remote sensing products depends on the precise calibration of the TIR channels. The methods of calibration for TIR channels of satellite sensors include prelaunch, onboard, and in-flight calibrations (Barnes et al. 1998, 2000; Minnis et al. 2002). In-flight calibration is used to validate the prelaunch

Corresponding author address: Bo Hu, Department of Human Resources and Education, China Meteorological Administration, Beijing 100081, China.
E-mail: hubo7178@yahoo.com.cn

DOI: 10.1175/2008JTECHA1139.1

and onboard calibrations. For in-flight calibration, an experimental site consisting of a large, homogeneous water body, such as Qinghai Lake (QHL) in China, is selected. When satellites view QHL, a field experiment is carried out over the lake to measure the upward radiance and brightness temperature with TIR radiometers (CE-312) and the atmospheric profiles with sounding balloons. The measured data are inputted into the atmospheric transfer model MODTRAN 3.7 (Acharya et al. 1998) to calculate the entrance pupil radiance and brightness temperatures. These are considered to be high values of the linear calibration curve, whereas the entrance pupil radiance of deep space is considered to be zero because it represents a low value of the linear calibration curve. Combining the two groups of entrance pupil radiance and brightness temperatures with the corresponding digital numbers (DNs), the calibration coefficients are obtained. Although there is a nonlinear component of a few percent in the very lower ranges of TIR channels, the prelaunch calibration experiments of the FengYun-2C (FY-2C) TIR channels have not measured the nonlinear calibration coefficients that are very difficult to assess from in-flight calibration experiments. Therefore, before the nonlinear calibration coefficients are determined in the prelaunch calibration experiments in the future FY-2 series satellite sensors, linear calibration is still adopted for FY-2C. In addition, Tong et al. (2008) test the effects of atmospheric profiles on the absolute radiometric calibration for TIR channels of FY-2C with MODTRAN 3.7, showing that in-flight absolute radiometric calibration coefficients are not sensitive to the water vapor profile. This is because the TIR channels avoid the absorption bands of water vapor and the MODTRAN 3.7 has sufficient precision to calibrate FY-2C TIR channels.

In China, QHL has been selected as a calibration site for TIR channels, including for FengYun-1C (FY-1C), FengYun-2B (FY-2B), and HaiYang-1 (HY-1; Wang et al. 2001; Tong et al. 2004a,b, 2005). QHL is located to the northeast of the Qinghai–Tibet Plateau in China, with the center approximately located at 36°45′N, 100°22′E. It covers an area of about 4635 km^2 at an elevation of 3196 m, and is considered an ideal calibration site for TIR channels based on the following reasons: 1) the water quality of QHL is very pure, with reflectivity of 4% and 1% for visible channels and TIR channels, respectively; 2) the surface temperature distribution of QHL is homogeneous with a range of less than 1 K; and 3) QHL is located at a high elevation location with pure atmospheric conditions, thus requiring less atmospheric correction for calibration. The in-flight calibration method has been used to calibrate the TIR channels successfully (Palmer 1993; Slater et al. 1996; Rong et al. 2007). This method, however, can only be carried out about twice every year, owing to the associated high labor requirements and monetary costs. The FY-2C with a multichannel scanning radiometer (MSR), launched in October 2004, has two split-window TIR channels covering 10.3–11.3 (TIR 1) and 11.5–12.5 (TIR 2) μm. The FY-2C is a Chinese operational geostationary meteorological satellite. The onboard calibration is implemented by inserting the calibration mirror into the optical path to measure the onboard blackbody regularly. Therefore, the calibration optical path does not include the entire optical path that is used to view earth targets. The onboard calibration system only calibrates the rear part of the entire optical path of the MSR on FY-2C, implying this is only a relative calibration. However, quantificational applications of remote sensing, such as temperature retrieval of the snow surface, are based on the high precision of absolute radiometric calibration (Key et al. 1997). To transfer from relative to absolute calibration, transform equations from onboard blackbody (OBB) temperatures to equivalent blackbody (EBB) temperatures are needed. Normally, these are developed during the prelaunch calibration experiments in the laboratory; however, the experiments cannot simulate the true orbital satellite states (Tong 2004). Thus, the transform equations for prelaunch satellite sensors cannot be used for those in orbit.

This paper describes the use of data during the operational mode of a satellite to develop the transform equations that are, as much as possible, based on the absolute radiometric calibration coefficients under various thermal states of the optical sensor system. The surface water temperatures of QHL measured by the automated hydrometeorological buoy (AHMB) system and the atmospheric profiles over QHL from National Centers for Environmental Prediction (NCEP) reanalysis data have been employed to calculate the absolute calibration coefficients for TIR channels of HY-1 and FY-2B successfully, which can substitute regular field experiments in QHL to obtain more frequent absolute radiometric calibration coefficients (Tong et al. 2004a,b, 2005). Combining the absolute radiometric calibration coefficients, onboard relative radiometric calibration coefficients, the temperatures of the primary, secondary, refraction, and calibration mirrors (collectively referred to henceforth as ''the mirrors'') on the optical sensors system, and the transform equations are developed to implement the onboard real-time absolute radiometric calibration for TIR channels of FY-2C.

2. Definition of EBB temperature

During operation, the TIR channels of FY-2C monitor the OBB to obtain the DNs every 3 h. The temperatures of the OBB and the mirrors are detected remotely. The EBB temperature is an imaginary temperature that is compared to the real OBB temperature. The EBB temperature is defined as follows: When the calibration mirror is inserted into the optical path of the MSR, the TIR sensors can detect the OBB to obtain a DN, and then the corresponding OBB temperature T_{OBB} can be detected remotely too. It is supposed that the environmental temperatures are the same as those when the OBB temperature is detected; there is an imaginary blackbody that passes through the entire optical path of the radiometer system, and the DN of the blackbody corresponds to that of the OBB. Therefore, the temperature of the imaginary blackbody is termed the EBB temperature T_{EBB} that is calculated as

$$T_{\mathrm{EBB}} \approx L_{\mathrm{EBB}} = G_w \times \mathrm{DN}_{\mathrm{OBB}} + I_w, \qquad (1)$$

where G_w and I_w represent the gain and offset for the entire optical path of the radiometer system, respectively, which are absolute calibration coefficients, and where $\mathrm{DN}_{\mathrm{OBB}}$ represents the digital number of OBB. Here, L_{EBB} represents the EBB radiance that can be converted directly to T_{EBB} via Planck's equation.

3. Method for EBB temperature

To develop the relationship between the T_{EBB} and temperatures of the OBB and the mirror, a large number of T_{EBB} is needed. The surface water temperatures of QHL measured by the AHMB system and the atmospheric profiles over QHL from the NCEP reanalysis data are employed to calculate the absolute calibration coefficients for the TIR channels of FY-2C. Tong et al. (2004a,b, 2005) adopted this method to successfully calibrate the TIR channels of HY-1 and FY-2B.

a. Remote sensing images of QHL from FY-2C

To calculate the calibration coefficients using the data from the AHMB in QHL and NCEP reanalysis data, we have to choose the cloud-free images of QHL from FY-2C first. The images of QHL at 0000, 0600, 1200, and 1800 UTC from 1 July to 30 September 2005 are verified to select 41 cloud-free images of QHL and to extract their corresponding DNs. Gray level and texture of clouds in the images are the most important characteristics to classify clouds. In this process, all of the images of visible and TIR channels and of QHL through the period are inspected visually in combination with corresponding meteorological observations to avoid choosing some images with cloud contamination. At last, the selected images are reviewed by experts to confirm they lack significant cloud contamination.

b. Data from AHMB and NCEP

According to the time of cloud-free images of QHL, the corresponding surface water temperatures of the lake measured from AHMB and the corresponding atmospheric profiles over QHL from NCEP reanalysis data are extracted. The QHL AHMB system is one component of the Weather and Environment Observation Systems in the China Radiometric Calibration Site for Remote Sensing Satellite. The AHMB continually measures five meteorological parameters, including atmospheric temperature, atmospheric pressure, humidity, wind speed, and wind direction, and two hydrological characteristics, including surface temperature and salinity, at a given fixed position from every April to October when the QHL is free from lake ice (Jin and Tan 2001). NCEP reanalysis data are globally gridded at $1° \times 1°$, including 26 vertical layers of various meteorological parameters that are available at 0000, 0600, 1200, and 1800 UTC (Kalnay et al. 1996). In this paper, the NCEP reanalysis data near 37°N, 100°E corresponding to the time of cloud-free images are considered representative of the humidity and temperature profiles above QHL.

c. Calculation of absolute calibration coefficients

After a selection based on the above steps, 41 groups of cloud-free images and their DNs of QHL and the corresponding surface water temperatures and atmospheric profiles are obtained. The surface water temperatures of QHL and atmospheric profiles are inputted into the atmospheric transfer model MODTRAN 3.7 to calculate the atmospheric transmittance and atmospheric path radiance. These are integrated over the spectrum response function of TIR channels of FY-2C to get the entrance pupil radiance and brightness temperatures when the satellite observes QHL. Comparing the entrance pupil radiance with the DNs, the absolute radiometric calibration coefficients of TIR channels are calculated as

$$L = G_w \times \mathrm{DN} + I_w, \qquad (2)$$

where L represents the entrance pupil radiance (mW $\mathrm{m}^{-2}\ \mathrm{sr}^{-1}\ \mathrm{cm}^{-1}$), DN represents the digital number, and G_w (mW $\mathrm{m}^{-2}\ \mathrm{sr}^{-1}\ \mathrm{cm}^{-1}\ \mathrm{DN}^{-1}$) and I_w (mW $\mathrm{m}^{-2}\ \mathrm{sr}^{-1}\ \mathrm{cm}^{-1}$) represent the gain and offset, respectively. The entrance pupil radiance of deep space is considered zero here. Figure 1 shows the 41 pairs of absolute radiometric calibration coefficients of TIR channels for FY-2C.

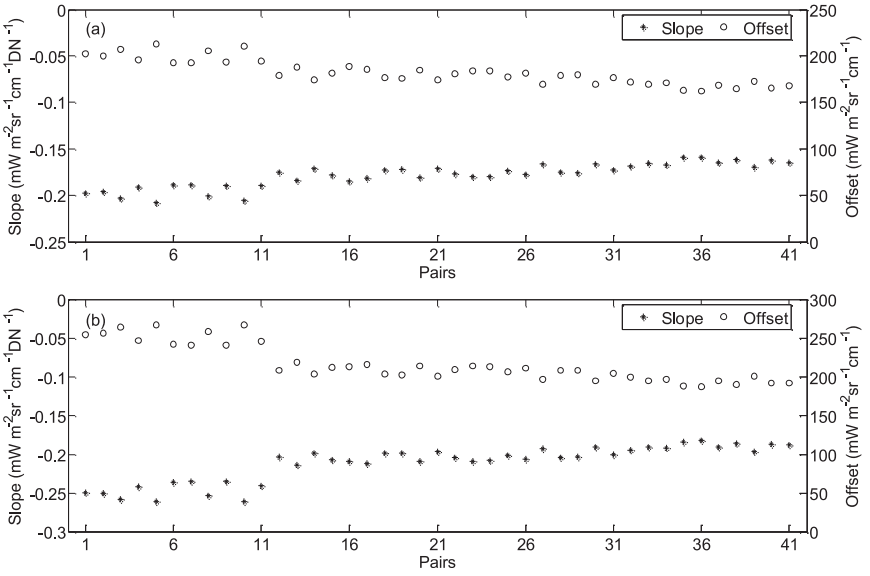

FIG. 1. Absolute radiometric calibration coefficients of TIR (a) 1 and (b) 2 of FY-2C.

d. Calculation of EBB temperature

After obtaining the 41 pairs of absolute radiometric calibration coefficients of TIR channels and corresponding DNs of OBB, the 41 EBB temperatures shown in Fig. 2 are calculated according to Eq. (1). These 41 EBB temperatures are the base of the transform equations from OBB to EBB temperatures.

4. Onboard absolute radiometric calibration

a. Transform equations between T_{EBB} and T_{OBB}

The calibration coefficients of TIR channels range with the temperatures of the mirrors. If the OBB temperatures can be transferred into EBB temperatures, the calibration for the entire optical path of the radiometer system can be implemented. Figure 3 shows that the maximum differences between T_{EBB} and T_{OBB} for TIR 1 and TIR 2 are −13.15 and −10.96 K, respectively; in other words, the differences of brightness temperature between absolute and relative calibration are −13.15 and −10.96 K, respectively.

In addition, the differences between T_{EBB} and T_{OBB} are not constantly varying with the onboard environmental temperatures. To investigate the relationship between T_{EBB} and T_{OBB} and onboard environmental temperatures, Fig. 4 shows the temperatures of OBB and the

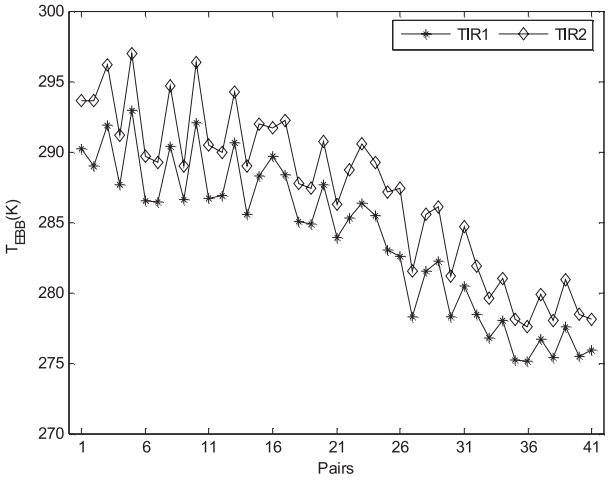

FIG. 2. EBB temperature for TIR 1 and TIR 2 using absolute radiometric calibration coefficients.

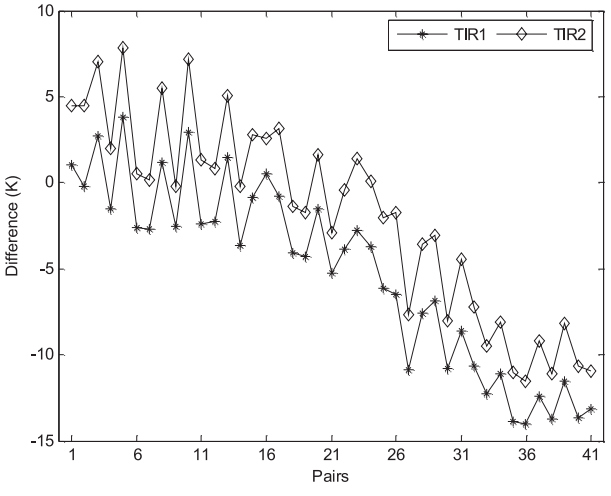

FIG. 3. Difference $T_{\mathrm{EBB}} - T_{\mathrm{OBB}}$ for TIR 1 and TIR 2 using absolute radiometric calibration coefficients.

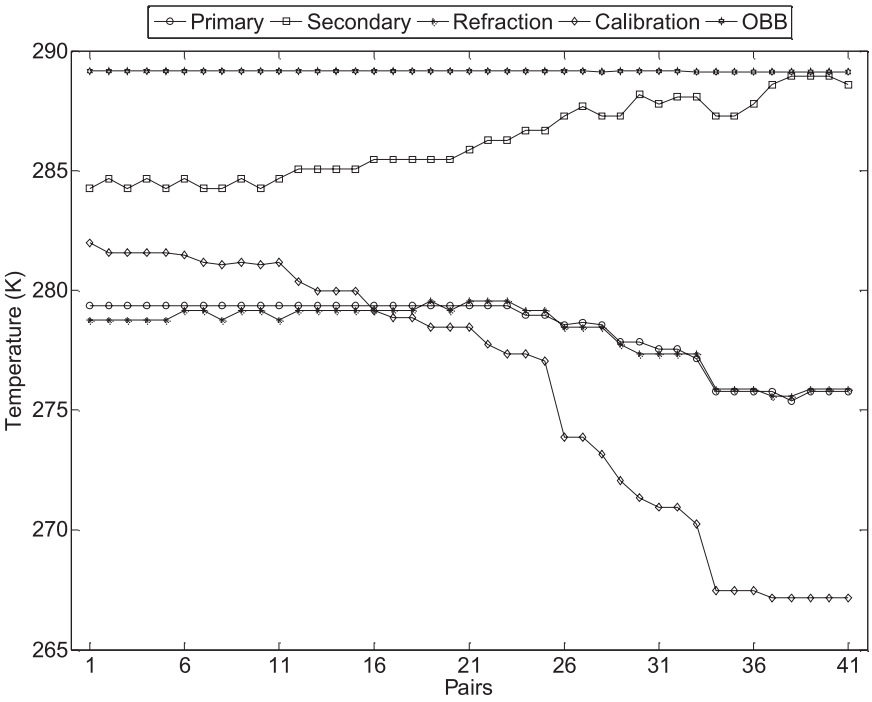

FIG. 4. Temperature of OBB, primary mirror, secondary mirror, refraction mirror, and calibration mirror.

mirrors corresponding to the 41 absolute radiometric calibration coefficients. This shows that during the operation of FY-2C, the temperatures of the primary and refraction mirrors rarely change, whereas the temperatures of the secondary and calibration mirrors range up to 4.3 and 14.8 K, respectively, for TIR 1 and TIR 2. The temperature changes of different mirrors are caused by the MSR itself and the relative position between the satellite and the sun. The OBB temperature is remotely fixed at 289.1 K.

There is a linear relationship between T_{EBB} and T_{OBB} and temperatures of various mirrors (Fig. 5). For TIR 1 of FY-2C, the correlation coefficients between T_{EBB} and T_{OBB} and temperatures of the mirrors are 0.88 ($p < 0.001$), -0.92 ($p < 0.001$), 0.83 ($p < 0.001$), and 0.94 ($p < 0.001$), respectively. For TIR 2 of FY-2C, the correlation coefficients between T_{EBB} and T_{OBB} and temperatures of the mirrors are 0.87 ($p < 0.001$), -0.91 ($p < 0.001$), 0.82 ($p < 0.001$), and 0.92 ($p < 0.001$), respectively. Therefore, the temperatures of various mirrors are considered as independent variables to fit $T_{\mathrm{EBB}} - T_{\mathrm{OBB}}$. To evaluate the fitted results, only 32 out of 41 groups of corresponding temperatures are adopted to develop fit equations, while the remaining 9 groups of corresponding temperatures are used for evaluation. These nine groups are selected based on the T_{EBB} and T_{OBB} that cover all of the observed ranges. Three different methods are employed to develop the fit equations. Respectively, T_p, T_s, T_r, and T_c (all in K) represent the temperature of the primary, secondary, refraction, and calibration mirrors, as

1) stepwise regressions with the independent variables of temperatures of the mirrors yield

$$\begin{aligned}\mathrm{TIR\,1}: T_{\mathrm{EBB}} - T_{\mathrm{OBB}} &= 1.628T_p + (-0.8898)T_s \\ &\quad + (-1.425)T_r + 0.6041T_c \\ &\quad + 26.0983. \end{aligned} \tag{3a}$$

$$\begin{aligned}\mathrm{TIR\,2}: T_{\mathrm{EBB}} - T_{\mathrm{OBB}} &= 3.235T_p + (-0.8935)T_s \\ &\quad + (-2.373)T_r + 0.4449\,T_c \\ &\quad + (-109.0907). \end{aligned} \tag{3b}$$

2) linear regressions with the independent variables of temperatures of the secondary mirror give

$$\mathrm{TIR\,1}: T_{\mathrm{EBB}} - T_{\mathrm{OBB}} = -3.1958T_s + 909.4482. \tag{4a}$$

$$\mathrm{TIR\,2}: T_{\mathrm{EBB}} - T_{\mathrm{OBB}} = -3.3054T_s + 944.1769. \tag{4b}$$

3) linear regressions with the independent variables of temperatures of the calibration mirror result in

$$\mathrm{TIR\,1}: T_{\mathrm{EBB}} - T_{\mathrm{OBB}} = 0.9351T_c + (-263.2648). \tag{5a}$$

$$\mathrm{TIR\,2}: T_{\mathrm{EBB}} - T_{\mathrm{OBB}} = 0.9751T_c + (-270.9571). \tag{5b}$$

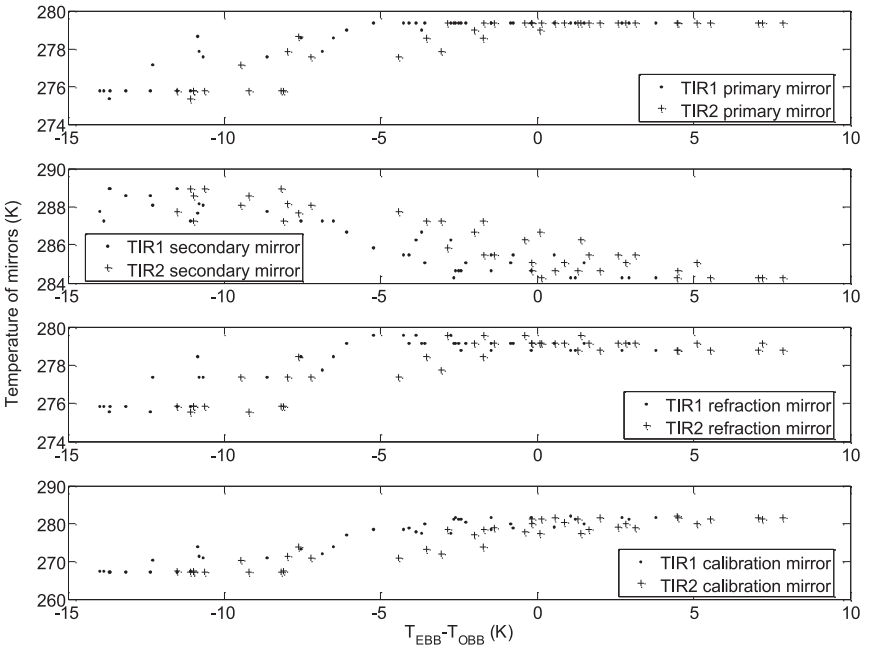

FIG. 5. Relationships between $T_{EBB} - T_{OBB}$ and temperatures of various mirrors for TIR 1 and TIR 2 of FY-2C.

b. *Validation of fitted results*

To evaluate the fitted results, T_{EBB} and T_{OBB} are calculated by using the remaining nine groups of corresponding temperatures based on Eqs. (3), (4), and (5). The differences between the fitted T_{EBB} and actual T_{EBB} are listed in Table 1. Although the three regression equations have different fitted results, they perform well to transfer the OBB to EBB temperatures. For example, for TIR channel 1, when (actual T_{EBB}) $-$ T_{OBB} is as large as -10.8 K at the eighth pairs, (fitted T_{EBB}) $-$ (actual T_{EBB}) are 1.55, -0.64, and 1.29 K for different regression equations, respectively. The root-mean-square (RMS) errors of the three different regression equations for TIR 1 channel are 1.47, 1.27, and 1.6 K, respectively, while the RMS errors of the three different regression equations for TIR 2 channel are 1.97, 1.81, and 2.14 K, respectively.

c. *Onboard absolute radiometric calibration*

During the operation of FY-2C, the temperatures of the OBB and the mirrors can be detected remotely. According to the transform Eqs. (3), (4), and (5), the EBB temperature is calculated, and then the onboard real-time absolute radiometric calibration can be carried out.

TABLE 1. Differences between the fitted T_{EBB} calculated by three regression methods and the actual T_{EBB} for TIR channels of FY-2C (unit: K).

	(fitted T_{EBB}) $-$ (actual T_{EBB}) TIR 1			(fitted T_{EBB}) $-$ (actual T_{EBB}) TIR 2		
Pairs	Stepwise regression	Secondary mirror	Calibration mirror	Stepwise regression	Secondary mirror	Calibration mirror
1	0.648	−0.082	0.207	−0.428	−1.23	−0.901
2	−1.885	−1.694	−2.68	−2.637	−2.474	−3.466
3	1.953	1.221	1.511	2.055	1.253	1.584
4	1.645	1.269	1.591	2.588	2.007	2.349
5	1.024	1.461	1.409	1.775	2.321	2.273
6	−1.206	−1.339	−1.391	−0.623	−1.026	−1.074
7	−1.736	−1.707	−1.991	−1.911	−2.277	−2.616
8	1.552	−0.641	1.296	2.856	−0.319	1.633
9	−1.007	−1.548	−1.263	−1.488	−2.55	−2.309
RMS error	1.465	1.273	1.599	1.974	1.808	2.142

5. Uncertainty of calibration

The transform equations are based on the absolute radiometric calibration coefficients calculated using the surface temperatures of QHL measured from AHMB and the matched atmospheric profiles over the lake from NCEP reanalysis data, which mainly accounts for the uncertainty of the calibration. Normally, the absolute radiometric calibration coefficients are calculated according to the field experiments at QHL. The uncertainty of the regular method, which is acceptable based on the calculated results of the TIR channels of HY-1, FY-1C, and FY-2B, consists of surface radiance of QHL, calculation of atmosphere radiative transfer, calculation of radiance of TIR channels, and extraction of DNs. For the calculation coefficients based on the surface water temperatures of QHL measured from AHMB and the corresponding atmospheric profiles over QHL from NCEP reanalysis data, the uncertainty mainly comes from measurement of water surface temperature, calculation of radiance of TIR channels, calculation of atmospheric radiative transfer, and extraction of DNs. These uncertainties are discussed in the following:

1) The uncertainty of measurements of surface water temperatures leads to the same uncertainty in the calculation of the entrance pupil radiance. The uncertainty of measurements of surface temperatures by AHMB in QHL is less than 0.3 K (Jin and Tan 2001).
2) In the calculation of the entrance pupil radiance, the water surface of QHL is considered as a ''blackbody'' with emissivity of unity. In the regular method, the water surface brightness temperature is measured by CE312. However, this water surface radiance is substituted by the water surface temperature measured by AHMB directly, which leads to the same uncertainty in the calculation of entrance pupil radiance. During August 2003, field experiments were carried out at QHL to calibrate the satellite sensors. CE312 was adopted to measure the water surface brightness temperatures that are compared with the corresponding surface temperatures measured by AHMB (Fig. 6). The data show that only 2 of the 10 absolute differences between surface brightness temperatures and surface temperatures reach about 0.6 K, whereas the remaining 8 of the 10 absolute differences are less than 0.5 K, with an RMS of 0.4355 K.
3) MODTRAN 3.7 is utilized to calculate the atmospheric transmission and atmospheric path radiance. The atmospheric profiles of NCEP reanalysis data substitute the atmospheric profiles measured by sounding balloon, which causes the uncertainty of calibration coefficients. During the field experiments at QHL in August 2003, 14 radiosonde measurements were conducted to obtain the atmospheric profiles over QHL. The corresponding atmospheric profiles of NCEP reanalysis data are extracted. The two types of atmospheric profiles are used to run MODTRAN 3.7 to calculate the entrance pupil radiance and brightness temperatures for TIR channels of FY-2C, respectively. The water surface brightness temperature is set as 15.1313 K. The results are shown in Fig. 7 (the units of entrance pupil radiance and brightness temperature are mW m^{-2} sr^{-1} cm^{-1} and K, respectively). In the 14 comparisons, the atmospheric profiles of NCEP reanalysis data substitute that of radiosonde measurements, which introduces the differences of entrance pupil radiance and brightness temperatures. For TIR 1 of FY-2C, the maximum difference of entrance pupil radiance is 2.002 mW m^{-2} sr^{-1} cm^{-1}, while the minimum difference of entrance pupil radiance is 0.0659 mW m^{-2} sr^{-1} cm^{-1}, with an RMS of 0.982 mW m^{-2} sr^{-1} cm^{-1}; the maximum difference of entrance pupil brightness temperature is 1.325 K, while the minimum difference of entrance pupil brightness temperature is 0.0438 K, with an RMS of 0.646 K. For the TIR 2 channel of FY-2C, the maximum difference of the entrance pupil radiance is 2.8227 mW m^{-2} sr^{-1} cm^{-1}, while the minimum difference of entrance pupil radiance is 0.0494 mW m^{-2} sr^{-1} cm^{-1}, with an RMS of 1.368 mW m^{-2} sr^{-1} cm^{-1}; the maximum difference of entrance pupil brightness temperature is 1.8135 K, while the minimum

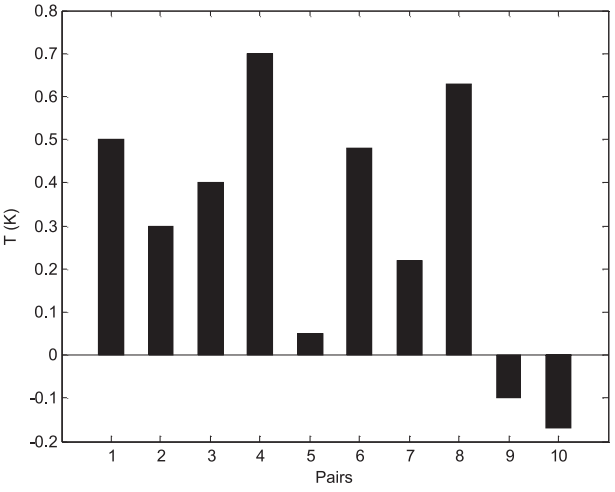

FIG. 6. The differences between water surface temperatures measured by AHMB and brightness temperatures measured by CE312 in 2003.

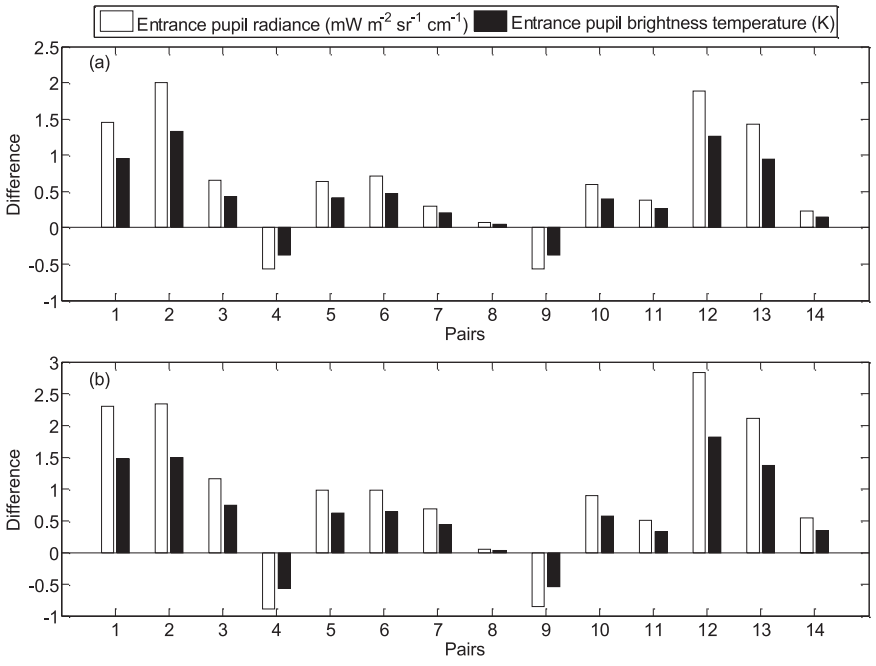

FIG. 7. Differences between entrance pupil radiance and entrance pupil brightness temperature of TIR (a) 1 and (b) 2 of FY-2C calculated using radiosonde measurements and NCEP reanalysis data.

difference of entrance pupil brightness temperature is 0.0319 K, with a RMS of 0.978 K. The total uncertainty of the onboard real-time absolute radiometric calibration of the TIR channels is calculated with the root sum of squares of all RMSs from different factors [Eq. (6)] that are used to evaluate the uncertainty of in-flight absolute radiometric calibration for visible channels (Slater et al. 1996);

$$\text{Uncertainty} = \sqrt{\sum_{i=1}^{n} \text{RMS}_i}. \qquad (6)$$

The fitting errors from T_{OBB} to T_{EBB} are not included in this uncertainty calculation again, because the fitting errors are supposed to be introduced by the nonlinear relationships between T_{OBB} and T_{EBB} that are caused by the calibration uncertainty. The uncertainties of TIR channels 1 and 2 of FY-2C are about 1.5 K and 2.1 K, respectively.

6. Conclusions

According to the analysis of T_{EBB} and T_{OBB} and the temperatures of primary, secondary, refraction, and calibration mirrors, T_{EBB} and T_{OBB} show a linear relation with the temperatures of the various mirrors, with correlation coefficients of 0.88 ($p < 0.001$), -0.92 ($p < 0.001$), 0.83 ($p < 0.001$), and 0.94 ($p < 0.001$) for TIR 1 and 0.87 ($p < 0.001$), -0.91 ($p < 0.001$), 0.82 ($p < 0.001$), and 0.92 ($p < 0.001$) for TIR 2, respectively. Combining the onboard relative calibration with in-flight absolute calibration at QHL, the transform equations between T_{EBB} and T_{OBB} are developed, and then the onboard real-time absolute radiometric calibration is implemented with an uncertainty of about 1.5 and 2.1 K for TIR 1 and TIR 2 of FY-2C, respectively. However, this method is based on at least 1 yr of operational data of FY-2C; therefore, this method can only be used beginning from the second year of operation of FY-2C. In addition, a physical model involving the optical system characteristics is needed to improve this statistical model developed in this paper.

Acknowledgments. J. Tong and S. Déry gratefully acknowledge support by the Canada Research Chair program of the government of Canada, the Natural Sciences and Engineering Research Council of Canada, the National Natural Science Foundation of China (NSFC-40675059), and the National Basic Research Program of China (2007CB714407). The paper benefited from the comments provided by two anonymous reviewers and the associate editor, Dr. Xianglei Huang.

REFERENCES

Acharya, P. K., and Coauthors, 1998: MODTRAN user's manual, versions 3.7 and 4.0. Hanscom AFB, Air Force Resource Laboratory, 80 pp.

Barnes, R. A., W. L. Barnes, C. H. Lyu, and M. J. Gales, 2000: An overview of the Visible and Infrared Scanner Radiometric calibration algorithm. *J. Atmos. Oceanic Technol.,* **17,** 395–405.

Barnes, W. L., T. S. Pangano, and V. V. Salomonson, 1998: Prelaunch characteristics of Moderate Resolution Spectroradiometer (MODIS) on EOS-AM1. *IEEE Trans. Geosci. Remote Sens.,* **36,** 1088–1100.

Jin, Y. M., and S. X. Tan, 2001: The meteorology auto-observation system in Qinghai Lake. *The Scientific Research Papers about China Radiometric Calibration Site for Remote Sensing Satellite*, K. Qiu, Ed., Oceanpress, 111–120.

Kalnay, E., and Coauthors, 1996: The NCEP/NCAR 40-Year Reanalysis Project. *Bull. Amer. Meteor. Soc.,* **77,** 437–471.

Key, J. R., J. B. Collins, C. Fowler, and R. S. Stone, 1997: High latitude surface temperature estimates from thermal satellite data. *Remote Sens. Environ.,* **61,** 302–309.

Minnis, P., L. Nguyen, R. D. Doelling, F. D. Young, F. W. Miller, and P. D. Kratz, 2002: Rapid calibration of operational and research meteorological satellite imagers. Part II: Comparison of infrared channels. *J. Atmos. Oceanic Technol.,* **19,** 1250–1266.

Palmer, J. M., 1993: Calibration of satellite sensors in the thermal infrared. *Proc. SPIE,* **1762,** 108–117.

Rong, Z. G., Y. X. Zhang, and F. M. Jia, 2007: On-orbit radiometric calibration of FENGYUN geostationary meteorological satellite's infrared channels based on sea-surface measurements in the South China sea. *J. Infrared Millimeter Waves,* **26,** 97–101.

Slater, P. N., S. F. Biggar, K. J. Thome, D. I. Gellman, and P. R. Spyak, 1996: Vicarious radiometric calibrations of EOS sensors. *J. Atmos. Oceanic Technol.,* **13,** 349–359.

Tong, J. J., 2004: The study on synthesis radiometric calibration methods for satellite sensors. Ph.D. dissertation, Department of Geography, Beijing Normal University, 120 pp.

——, K. M. Qiu, and X. W. Li, 2004a: Absolute radiometric calibration for thermal infrared channels of FY2B by using NCEP reanalyzed data in Qinghai lake. *IEEE Geosci. Remote Sens. Symp.,* **6,** 3960–3962, doi:10.1109/IGARSS.2004.1369994.

——, ——, and ——, 2004b: Absolute radiometric calibration for thermal infrared channels of HY-1/COCTS by using Qinghai Lake. *IEEE Geosci. Remote Sens. Symp.,* **6,** 3963–3965, doi:10.1109/IGARSS.2004.1369995.

——, ——, and ——, 2005: New method of in-flight absolute calibration for thermal infrared channels of satellite sensors. *J. Infrared Millimeter Waves,* **24,** 275–280.

——, Y. Zhang, B. Hu, K. M. Qiu, J. M. Xv, and Z. G. Rong, 2008: Affect of atmospheric profiles on the absolute radiometric calibration for thermal infrared bands of FY2C. *J. Infrared Millimeter Waves,* **27,** 337–341.

Wang, W. H., Z. G. Rong, Y. X. Zhang, and X. Q. Hu, 2001: Radiometric calibration for the thermal channels of FY-1C and FY-2B. *The Scientific Research Papers about China Radiometric Calibration Site for Remote Sensing Satellite* K. Qiu, Ed., Oceanpress, 307–319.